Article

https://doi.org/10.1007/s12303-019-0050-7
pISSN 1226-4806 eISSN 1598-7477

Geosciences Journal GJ

Genesis of the Heneshk IOCG deposit, Iran: magnetite mineral chemistry and sulfur isotope

Morteza Mizan[1]* and Xiao-Wen Huang[2]

[1]Department of Earth Sciences, College of Sciences, Shiraz University, Shiraz, Iran
[2]State Key Laboratory of Ore Deposit Geochemistry, Institute of Geochemistry, Chinese Academy of Sciences, Guiyang 550081, China

ABSTRACT: The Heneshk Fe ± Cu deposit, a metamorphosed IOCG (Iron Oxide Copper Gold) is situated in Sanandaj–Sirjan Zone, SW Iran. Mineralization occurs as two stratabound 'U' shape ore bodies, hosted by a meta-dolomite member of a metamorphic complex. The ore and gangue minerals comprise magnetite, chalcopyrite, hematite, martite, mushketovite, pyrite, barite, calcite, dolomite, and quartz. The successive mineral assemblage formed in the five paragenetic stages (I to V) during an ongoing deformation regime from the plastic to the brittle deformation regime. The mineralization stages comprise stage I, III, and IV. Stage I–III and IV formed in the plastic and the brittle deformation regime by the metamorphic processes in a shear zone, respectively. The concomitant alteration products of these stages comprise sodic, Fe, K, hydrolytic and silicification. The sodic and Fe alterations occur as a pre-mineralization stage and each mineralization stage is accompanied by K and hydrolytic alterations. A late barite-calcite-quartz assemblage (stage V) overprinted on the previous stages (I to IV). Stage I mineralization formed at a depth of ~10 km and temperature of ~300 °C (a high pressure-low temperature environment). The partitioning and substitution of the Mg, Al, Ti, Ni, Cr, Mn, Si, and Zn elements increased in this relatively higher pressure environment cause of the highest concentrations of the Al, Ti, Ni, Cr, and Zn, in comparison with metamorphic magnetite. The mineral chemistry of the Heneshk magnetite (average elemental concentrations) is in accordance with the metamorphic magnetite and can consider as a pure magnetite with the low elemental concentration. Also, the $\delta^{34}S_{H_2S}$ Heneshk mineralized fluid ranges between 39.8 to 40.6‰, indicating the contribution of the paleo-evaporates. The pleo-evaporates leached from the older strata during metamorphism, and their precipitation in the form of the sulfide minerals occurs through the TSR (Thermochemical Sulfate Reduction) mechanism.

Key words: Heneshk IOCG, metamorphic magnetite, magnetite mineral chemistry, elemental substitutions, paleo-evaporates

Manuscript received November 17, 2018; Manuscript accepted July 9, 2019

1. INTRODUCTION

Heneshk Fe ± Cu deposit, economically one of the largest iron deposits of Dehbid district, with controversial genetic aspects, is located approximately 4 km north-east and 4.8 km south-east of the Heneshk and Goushti villages respectively (Fig. 1b). Fe and Cu metals merely occur as magnetite-hematite and chalcopyrite minerals. First assessment of the Heneshk mine went back to 1977 by Alric and Virlogeus, proposed a metamorphic origin. Later, Rajabzadeh and Rasti (2017) proposed a magmatic-hydrothermal origin (namely, Goushti deposit) and Sabzehi (2013) proposed an IOCG (Iron Oxide Copper Gold) type, linked with metamorphic processes. This deposit even classified by Nabatian et al. (2015) as a volcano-sedimentary deposit. Despite the considerable complexity of the genetic aspects of the Heneshk deposit, caused by metamorphism and simultaneous magmatism in Dehbid region, since the 1970s, a few studies have performed on this deposit and each study tends toward a piece of evidence for unraveling the genetic aspects of the mine.

Both magnetite mineral geochemistry and sulfur stable isotope studies are reliable methods for understanding the ore-forming processes including source, transporting, and precipitation mechanism of the ore components and mineralization fluid. Recently, the magnetite mineral geochemistry, that is elemental substitutions-concentrations (namely, Al, Co, Cr, Ga, Ni, Mg, Mn, Sn, Ti, V, Zn) as a function of source rock or magma composition, temperature-pressure ranges, cooling rate, oxygen fugacity, sulfur fugacity, and silica-sulfide activity, was subjected to studies by several

*Corresponding author:
Morteza Mizan
Department of Earth Sciences, College of Sciences, Shiraz University, Shiraz, Iran
Tel: +98-9107030903, E-mail: mizan.morteza@gmail.com

researcher (Dupuis and Beaudoin, 2011; Nadoll et al., 2012, 2014; Dare et al., 2014; Huang et al., 2018). These studies provide discriminate diagrams to distinguished different deposit types or subtype and impose a major constraint on the mineralization fluid sources and geological environments (Dupuis and Beaudoin, 2011; Dare et al., 2014; Nadoll et al., 2014; Huang et al., 2018). Also, the conventional sulfur stable isotope analysis has utilized for six decades for unraveling the source of the sulfur, transportation and precipitation mechanisms for deposits (Ohmoto and Goldhaber, 1997; Shanks, 2013). Among different deposit types, IOCGs are characterized by voluminous magnetite-hematite and abundant sulfide minerals as main component of the ore (Williams et al., 2005; Groves et al., 2010; Barton, 2014) by which, the magnetite mineral geochemistry and sulfur stable isotope can be used as an alternative means for unraveling the genetic aspects and geological environments of this deposit type.

Different genetic models, proposed by several authors reflect the complexity of the genetic aspects of the Heneshk deposit. This deposit is hosted by a metamorphic complex, located in a shear zone (Kowli Kosh-Goushti shear zone) (Sarkarinejad et

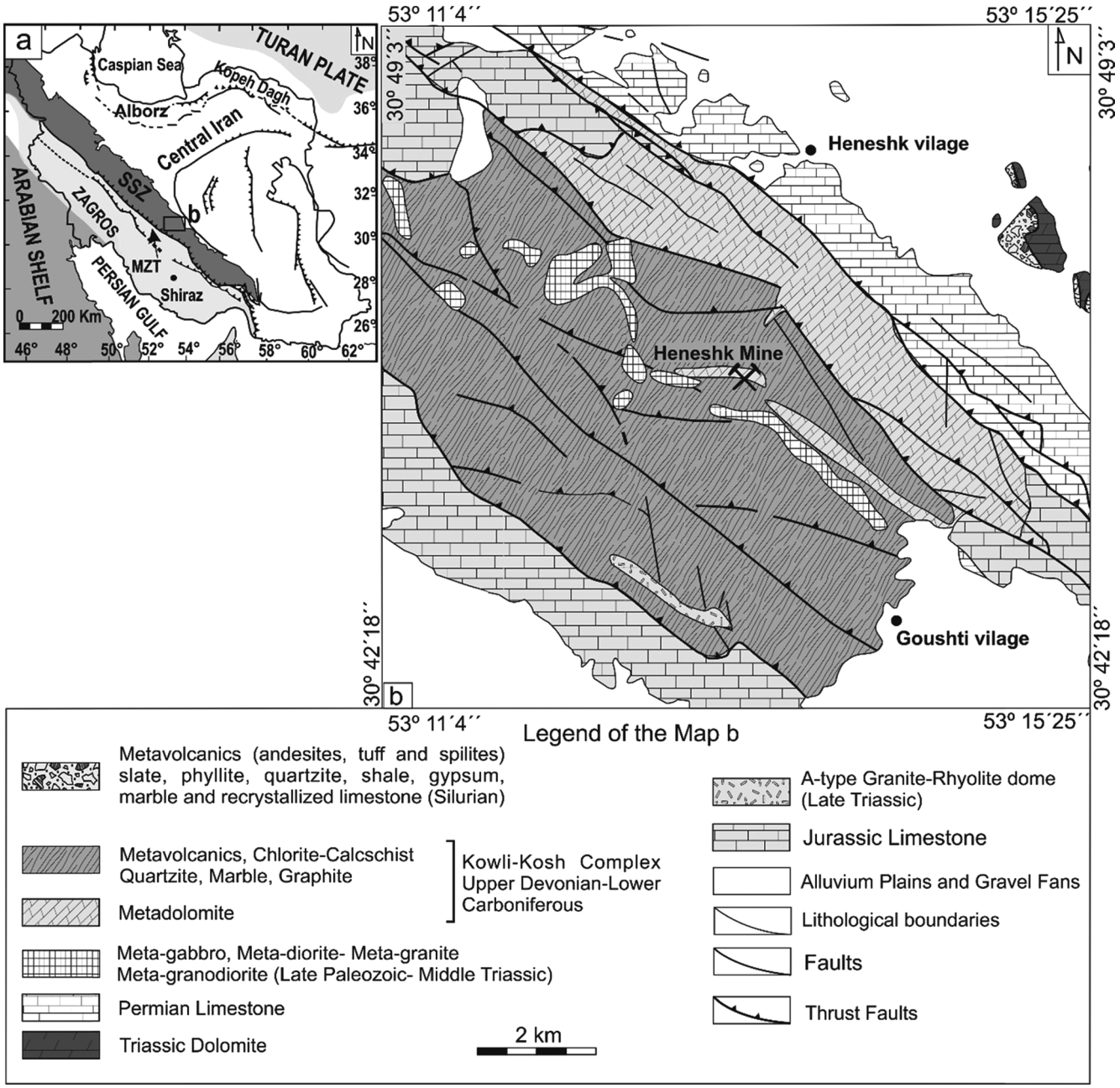

Fig. 1. (a) Geological map of Iran with different tectonostratigraphic units (Berberian and King, 1981). The quadrangle is represented the geologic setting of the Dehbid district. (b) Modified geological map of the Dehbid district (after Houshmandzadeh et al., 1975; Shahidi et al., 1999). Abbreviations: SSZ = Sanandaj-Sirjan Zone, MZT = Main Zagros Thrust.

al., 2008; Samani, 2017) and ore characterize by plastic and brittle deformation textures-structures which can interpret as primary (metamorphogenic) or secondary overprinted textures. The geology, mineralogy, alteration facies, magnetite mineral geochemistry, partitioning of elements into the magnetite phase, mineralization environment and temperature-pressure range of the mineralization event have not subjected to a comprehensive study since the discovery of this mine. In this article, we attempt to investigate the mineralogy, alteration facies, pressure-temperature range of the main mineralization event, relationship between the mineralization and metamorphism, source of the sulfur, ore-forming environment, the partitioning of elements into the magnetite phase in an ore-forming environment, and the genetic model based on detail petrographic studies (textural interpretation), sulfur stable isotope study and Electron probe microanalysis (EPMA) analysis of the magnetite.

2. REGIONAL GEOLOGY

The Heneshk deposit is situated at north-east of Shiraz city, Fars province, in Dehbid district, part of Sanandaj–Sirjan Zone (SSZ) (Fig. 1a). The SSZ stretches 1500 km long and 200 km width from north-west to south-east of Iran (Mohajjel et al., 2003; Fig. 1a) and poly-phase metamorphism and extensive magmatism through its geological records characterizes this zone (Mohajjel et al., 2003; Fergusson et al., 2016). The Main Zagros Thrust (MZT) confines this zone to the west, and it is situated at the margin of Central Iranian zone (Hassanzadeh and Wernicke, 2016; Fig. 1a). Stratigraphic successions in Dehbid district comprise Silurian, and upper Devonian–Lower Carboniferous metamorphosed rock sequences and Permian to Jurassic carbonate rock strata (Fig. 1b).

The Heneshk deposit is hosted by upper Devonian–Lower Carboniferous Kowli-Kosh metamorphic complex which comprises basinal rift sequences (Houshmandzadeh et al., 1975; Fig. 1b). This complex constitutes metavolcanics, chlorite-calcschist, quartzite, marble, graphite, and meta-dolomite members (Fig. 1b) which primarily comprises greywacke, sandstone, arkose, carbonate (limestone-dolomite strata), and shale units with interbedded basalt-rhyolite lava (bimodal volcanism), undergone amphibolite facies metamorphism and deformation (regional metamorphism), in late Triassic (Houshmandzadeh et al., 1975; Alric and Virlogeus, 1977).

Two groups of intrusions intruded to the Kowli-Kosh complex during the late Paleozoic to late Triassic. The first group of intrusions emplaced during the late Paleozoic–middle Triassic time interval which constitutes meta-gabbro, meta-diorite, meta-granodiorite, meta-granite and subsequently metamorphosed and deformed during the late Triassic (Houshmandzadeh et al., 1975; Fig. 1). These intrusions had an alkaline affinity and emplaced during rifting event. The second group of intrusions emplaced in the late Triassic age after the metamorphic event and comprises A-type granite-rhyolite dome without deformation (Houshmandzadeh et al., 1975; Fig. 1).

3. ORE DEPOSIT GEOLOGY AND DEFROMATIONAL HISTORY

The Heneshk deposit is hosted by a meta-dolomite member of the Kowli-Kosh complex as two stratabound ore bodies (Fig. 2). Upper and lower stratigraphic members of the meta-dolomite are upper and lower chlorite schist members, respectively (Fig. 2) with a greenish color in the mining area (Fig. 3a). These two members have gradational contact with the meta-dolomite (Fig. 3a). The meta-dolomite member is characterized by dolomite sublayers with an NW-SE trend and 45° dip to the SE. These sublayers, variably have several centimeters to meters thickness, with cavity-vuggy texture and bright-dark brownish color (Figs. 4d and g). The dark brownish color of the sublayers is caused by abundant iron oxide. Mineralization occurs as two 'U' shape ore bodies, lying one ore body top of the other, separating out by an altered meta-dolomite (Figs. 2 and 3b). The ore bodies have 400 m lengths, 50 to 100 m widths, with at least 100 m in depths (Fig. 2). The middle sections of the ore bodies have a maximum thickness and depths. From the center of the ore bodies towards the two end sections, in both horizontal and cross-section plane view, a distinct thinning occurs (Figs. 2 and 3b). The extensive deformation arrays of the meta-dolomite and ore are reflected in the concordant shape of the ore bodies (Fig. 2) with NW-SE trends and 45° dip to the SE, the identical to the host rock. However, these ore bodies traverse the upper and lower meta-dolomite sub-layers, especially in the middle sections.

Structurally, the Heneshk deposit is located in a shear zone (Sarkarinejad et al., 2008; Samani, 2017), having both the plastic and the brittle deformation structures-textures with the ore bodies and the meta-dolomite host rock. The lineation-foliation of the ore and meta-dolomite comprise the deformation arrays of the shear zone. This zone is characterized by mylonitic-ultramylonitic rocks with generally NW-SE strike similar to the meta-dolomite strata trends. The characteristics of these rocks in the hand species is a distinct foliation due to the mylonitization. In the peripheral sections to the ore bodies, mylonitic rocks with sparse porphyroclasts occur and gradually transform into the ultramylonitic rocks with any porphyroclasts across and along with the ore bodies. The deformation textures-structures of the Heneshk deposit can divide into the D_1 and D_2 deformation regime, based on their relative timing (Table 1). The recognized D_1 deformation textures-structures, with mylonitic and ultramylonitic

https://doi.org/10.1007/s12303-019-0050-7

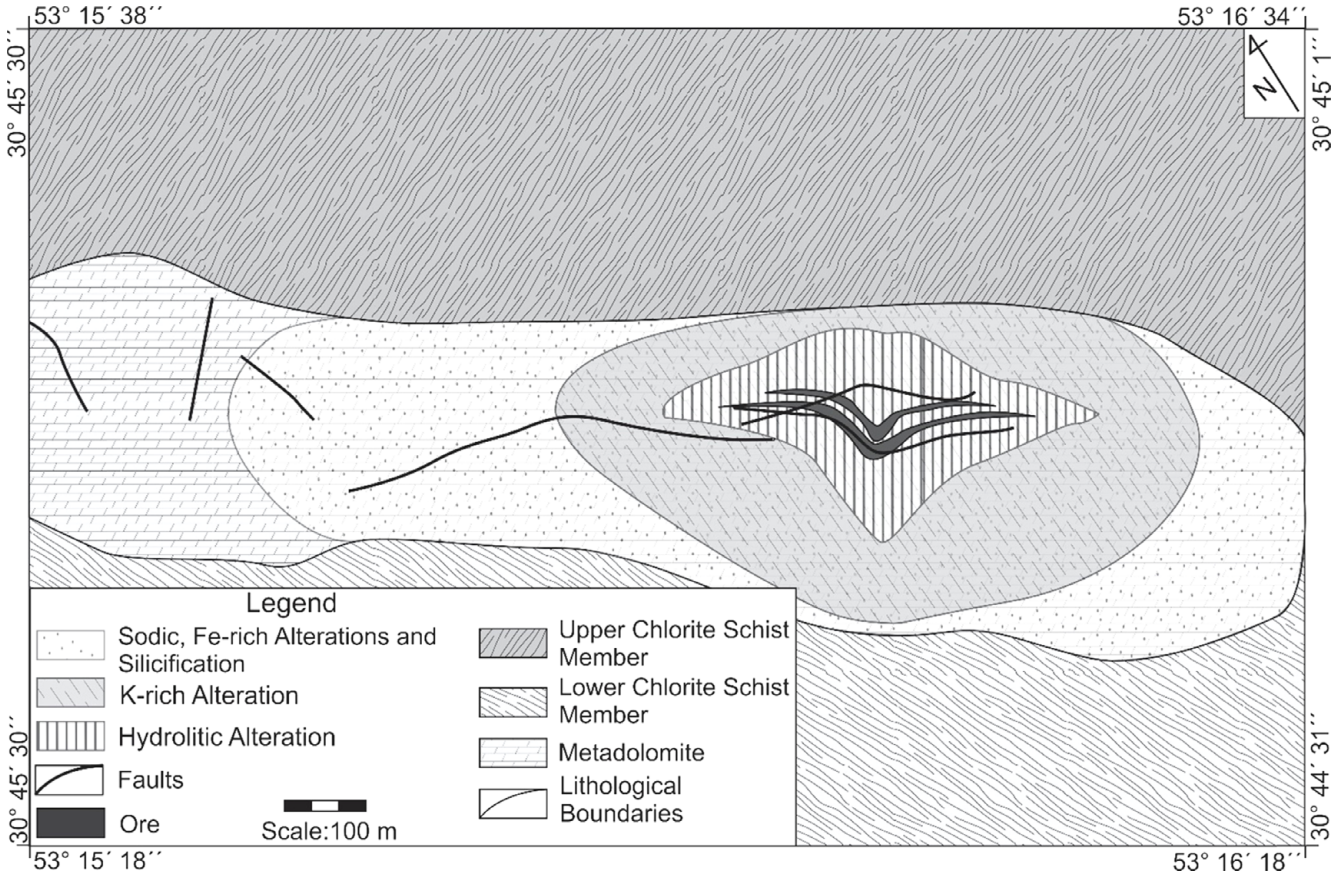

Fig. 2. Geological map of the Heneshk deposit.

rocks comprise mylonites, rootless folds, S=C structures, implosion breccia, folding, and foliation. All of these textures-structures are part of the plastic deformation regime. The overprinted D_2 deformation textures-structures on the D_1 fabrics are characterized by abundant extensional veins, developed in the brittle deformation processes, by the late extensional processes during metamorphism. Also, in the late extensional processes, several faults formed with the ore bodies without offsetting. Furthermore, the folding of the meta-dolomite, part of the D_1 deformation regime, is reflected in the 'U' shape geometry of the two ore bodies (Fig. 2). So, the mining area is characterized by the plastic and a late brittle deformation regime (Table 1).

4. MINERALIZATION AND PARAGENETIC SEQUENCE

Petrography studies were performed on the thirty-five sections, which comprise twenty thin, ten polish, and five thin-polish sections. These sections were acquired from the meta-dolomite host rock and ore bodies. Based on petrographic studies, the Heneshk Fe-Cu mineralization constitutes abundant magnetite, chalcopyrite, accessory specular hematite, mushketovite, and rare pyrite. Mineralization occurs as two massive 'U' shape ore bodies, and the main ore component consists of magnetite-chalcopyrite in a silicified carbonate matrix (Figs. 4b and 5b). The gangue minerals constitute abundant quartz, calcite, dolomite, and minor barite (Figs. 4i and 5a–d, f). Furthermore, disseminated and vein type of the mineralization occur with the two end sections of the ore bodies as a replacement and open space filling forms, respectively (Figs. 3d, f, and 4f, h, i). Across these two end sections toward the meta-dolomite in an NW-SE strike, the iron grade and relative abundance of the Fe-oxide minerals decrease, as a characteristic of a transition, from massive to disseminated ore. However, in the middle sections of the ore bodies, the meta-dolomite host rock has a sharp contact with massive ore without disseminated ore (Figs. 3b and d). Moreover, infill forms occur with massive ore, especially for sulfide minerals (Figs. 4a–c and e). The Heneshk mineralization formed in the three stages in a complex paragenetic sequence (Table 1). The paragenetic sequence consists of five distinct stages, and each stage is characterized by different mineralogy, alteration products, and deformation textures-structures (Table 1). The ore-gangue minerals display a close temporal-spatial relationship with deformation elements of the meta-dolomite host rock and ore as well (D_1 and D_2 deformation textures and structures) (Figs. 4a, b, d, e, and 5h).

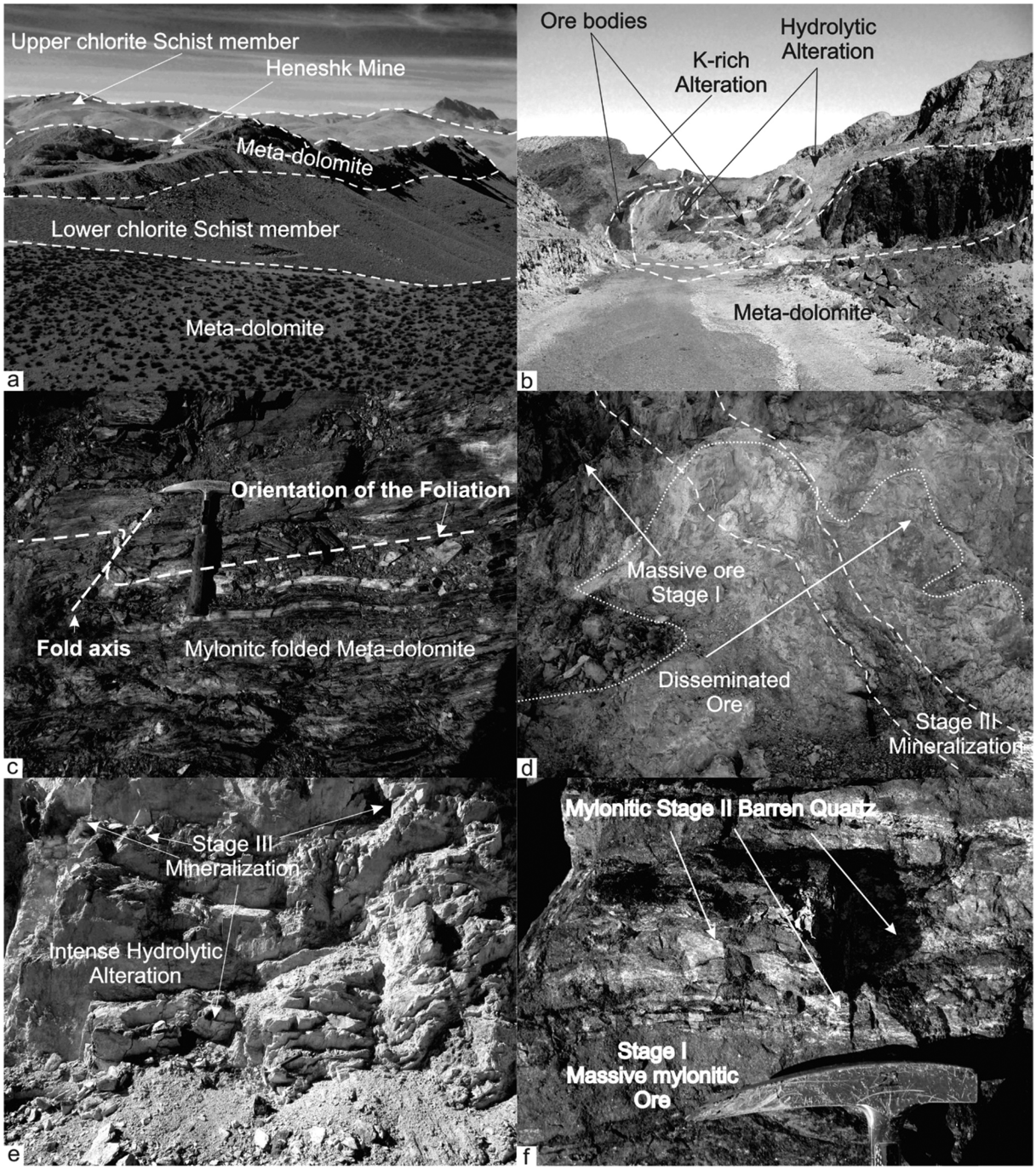

Fig. 3. (a) The Heneshk deposit is situated between the upper and lower chlorite schist members of the Kowli-Kosh complex with a meta-dolomite host rock. (b) The two massive 'U' shape ore bodies are accompanied by the K (grey) and hydrolytic (white) alterations with a meta-dolomite host rock. (c) This figure represents the folded mylonitic meta-dolomite with white color due to the abundant of the chlorite mineral (sodic alteration). The meta-dolomite host rock is displaying the orientation of the foliation. (d) This figure represents the cross-cutting relationship between stage I (massive ore) and stage III mineralization (vein type of mineralization). (e) This figure represents the intense hydrolytic alteration type (white) and the stage III mineralization (black hematite-enriched veins). (f) This figure represents the cross-cutting relationship between stage I mylonitic ore (grey) and stage II barren quartz veins (white) with vein textured clasts structures.

4.1. Paragenetic Sequence

The paragenetic sequence of the Heneshk deposit is represented in Table 1. Five paragenetic stages are recognized based on crosscutting relationships, mineralogy, alteration products, and deformation texture-structures (Table 1). Among these stages, stage I constitutes more than 95 vol. percent of the ore bodies and include more than 90 vol. percent of the magnetite ore

https://doi.org/10.1007/s12303-019-0050-7

Table 1. The paragenetic sequence of the Heneshk deposit with the first (D_1) and the second (D_2) deformation regime

Minerals and alteration types	Pre-Mineralization (D_1)	Stage I (Mineralization) (D_1)	Stage II (D_1)	Stage III (Mineralization) (D_1)	Stage IV (Mineralization) (D_2)	Stage V (D_2)
Sodic & Fe-rich	▬					
Hydrolytic		▬		▬	▬	
K-rich		▬		▬	▬	
Silicification			▬		▬	
Magnetite		▬ ▬ ▬		▬	▬	
Hematite	▬	▬ ▬		▬	▬	
Chalcopyrite		▬				
Pyrite		▬				
Quartz			▬		▬	▬
Barite						▬
K-feldspar		▬		▬	▬	
Biotite		▬		▬	▬	
Albite	▬					
Sericite		▬		▬	▬	
Chlorite	▬					
Ankerite	▬					
Goethite	▬					
Calcite	▬					

component (Figs. 4a–c). Economically, other stages have subordinate roles to the stage I mineralization. Ore and gangue minerals with these five stages are displaying open space filling, replacement, and deformation textures-structures. Replacement textures comprise a depositional sequence (enrichment of the Fe component in oxide minerals), non-matching walls, pseudomorphs, islands of un-replaced of the host rock, gradational boundaries, a concave surface, no offset along intersecting veins, transection an older structure transect by the younger one. The open space filling textures comprise euhedral grains, cavity and vugs, matching walls, symmetrical banding, infills, and fine-grained minerals on the wall and coarser one in the center. These stages (I to V) formed in the D_1 and D_2 deformation regime. Stage I–III and IV–V formed in the plastic (D_1) and brittle (D_2) deformation regime, respectively.

4.1.1. Stage I

Economically and volumetrically, stage I is the main mineralization stage in the Heneshk deposit. More than 95 vol. percent of the ore bodies constitute stage I mineral assemblages which comprise abundant magnetite, chalcopyrite, accessory hematite, martite, mushketovite, and rare pyrite (Table 1; Figs. 4a–c, and 5a–d, h). The Fe-oxide and sulfide minerals formed as massive or disseminated forms, displaying replacement and open space filling textures (Figs. 3d, f, 4a–d, h, and 5a–c, i). The sulfide minerals only occur with the massive ore (Fig. 4c) and randomly, developed through the ore bodies (Figs. 4a and c). Open space filling textures comprises cavities-vugs, infills, and euhedral grains (Figs. 4a, c, and 5a–c). Euhedral mineral grains comprise magnetite and specular hematite (Figs. 5a and c). Chalcopyrite and pyrite occur as infill components of the remnant vugs-cavities of the massive ore (Figs. 5a and c). Replacement textures are pseudomorphs, a young mineral transect old structure, gradational boundaries, and islands of un-replaced wall rock. The Fe-oxide ore minerals such as martite and mushketovite are displaying pseudomorph texture and the island of the un-replaced meta-dolomite occurs with the ore (Figs. 4a, c, and 5a, b). The sulfide minerals (old structure) are transected and replaced by late Fe-oxide ore minerals (young structure) with gradational boundaries (Figs. 5c and d). The mineral deposition sequence of this stage comprises early magnetite, late hematite and last magnetite phases (Table 1). Mushketovite (magnetite after hematite) and martite ore minerals occur with this sequence as replacement forms of the early magnetite phase (Figs. 5c and d). The early magnetite grains have ~0.7 to 0.2 mm range in size (Figs. 5a and c). After this mineral assemblage, sulfide minerals formed as infills of the remnant cavities-vugs of the ore (Figs. 4c and 5a), characterizing with euhedral grains with ~1 cm to ~0.5 mm range in size. Then, these sulfide minerals are fractured and cemented by early magnetite and late hematite phases (Table 1). The late magnetite and hematite mineral assemblages are fine-grained anhedral (~> 0.1 mm) phases as replacement forms (Fig. 5d). Furthermore, D_1 deformation textures-structures including mylonites and foliation characterizes stage I mineralization (Figs. 4a–c). The ore minerals of this stage, occurring with the meta-dolomite host-rock have a close temporal-spatial relationships

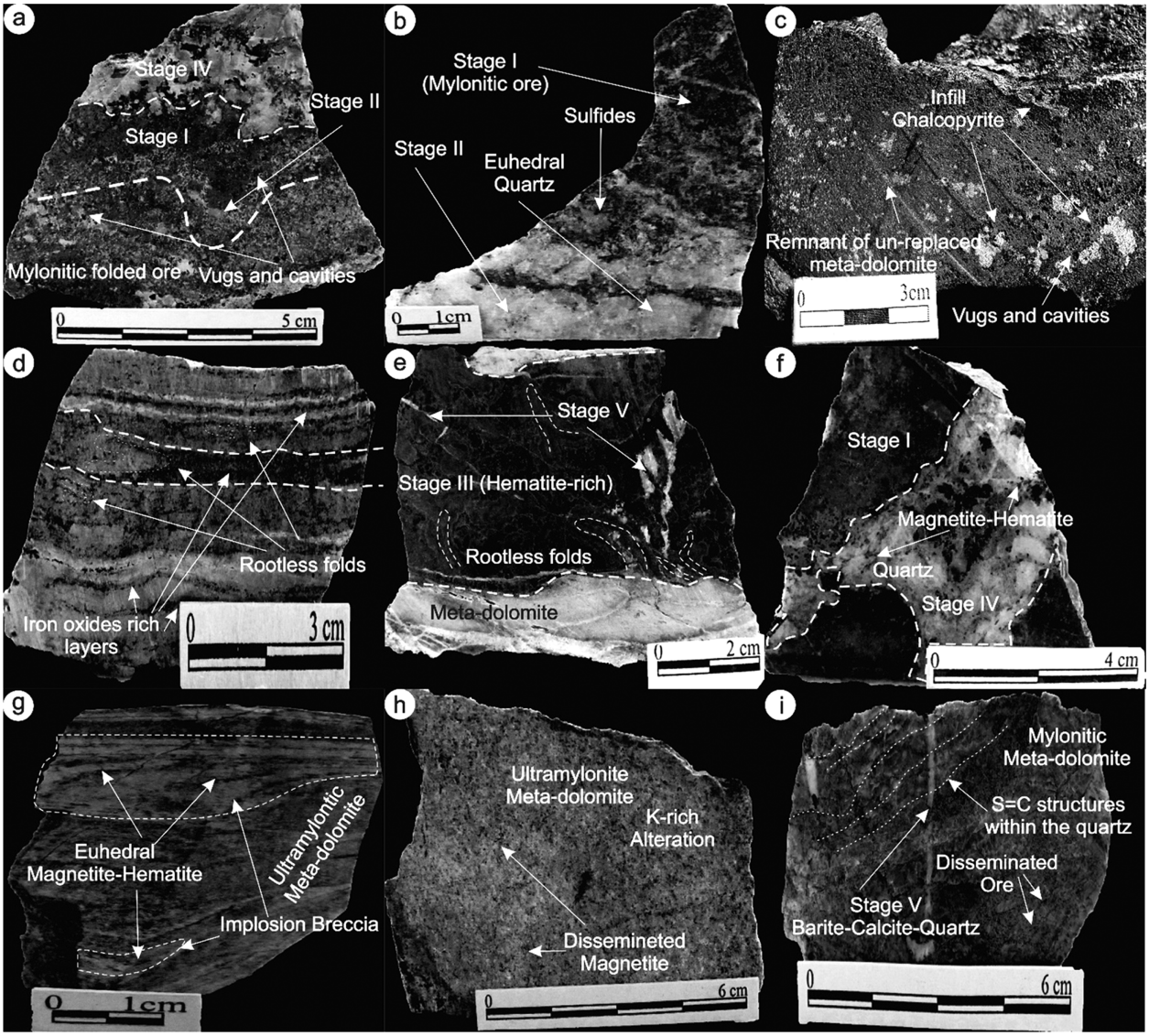

Fig. 4. (a) The mineralized veins (white, stage IV) transects mylonitic folded ore (stage I and II mineral assemblages), and the ore is characterized by the cavities and vugs (black). (b) Stage II (white barren euhedral quartz) transects stage I mylonitic ore (dark-grey). (c) This figure represents stage I mylonitic ore (magnetite-chalcopyrite) with the remnants of un-replaced meta-dolomite (grey). (d) This figure represents rootless fold structures of the meta-dolomite, lying in the iron oxide-rich matrix (black). (e) This figure represents hematite-rich veins (stage III) with rootless fold structures. (f) Magnetite rich veins (stage IV) transects stage I mylonitic ore (stage I). (g) This figure represents the ultramylonitic meta-dolomite with implosion breccia structures. Each structure (dark-grey) is characterized by a dark layer of the magnetite-goethite with elongated 'S' shape geometry. (h) This figure represents the ultramylonitic meta-dolomite with disseminated ore and concomitant K alteration type (light-grey). (i) The barite rich vein (stage V) transects the silicified mylonitic meta-dolomite with S=C structures and disseminated ore.

with deformation structures-textures, including mylonites, implosion breccia, S=C structures, rootless folds, folding and foliation (Figs. 3c, f, 4a, d, e, g, and 5c–e, h). The mylonitic texture of the meta-dolomite is characterized by carbonate grains size reduction, and foliation of the host rock with dark and light layering appearance (Figs. 3c, 4d, g, and 5h, i). The light and dark layers mainly constitute carbonate and hematite (major)-magnetite (minor) phases, respectively (Fig. 5h). Also, the magnetite and hematite occur with the fine-grained matrix and porphyroclasts of the mylonitic meta-dolomite as anhedral-euhedral grains (Figs. 5e, f, e, i). The porphyroclasts consist of quartz, magnetite, hematite, and carbonate phases (Fig. 5e). The rootless folds structures are characterized by folded white meta-dolomite, lying in the enriched Fe-oxide layers (Fig. 4d). Furthermore, the implosion breccia structures filled with euhedral magnetite and goethite (Fig. 4g). Within the implosion breccia structures, the magnetite minerals are surrounded by goethite phase, displaying the depositional sequence texture (enrichment in the Fe element)

https://doi.org/10.1007/s12303-019-0050-7

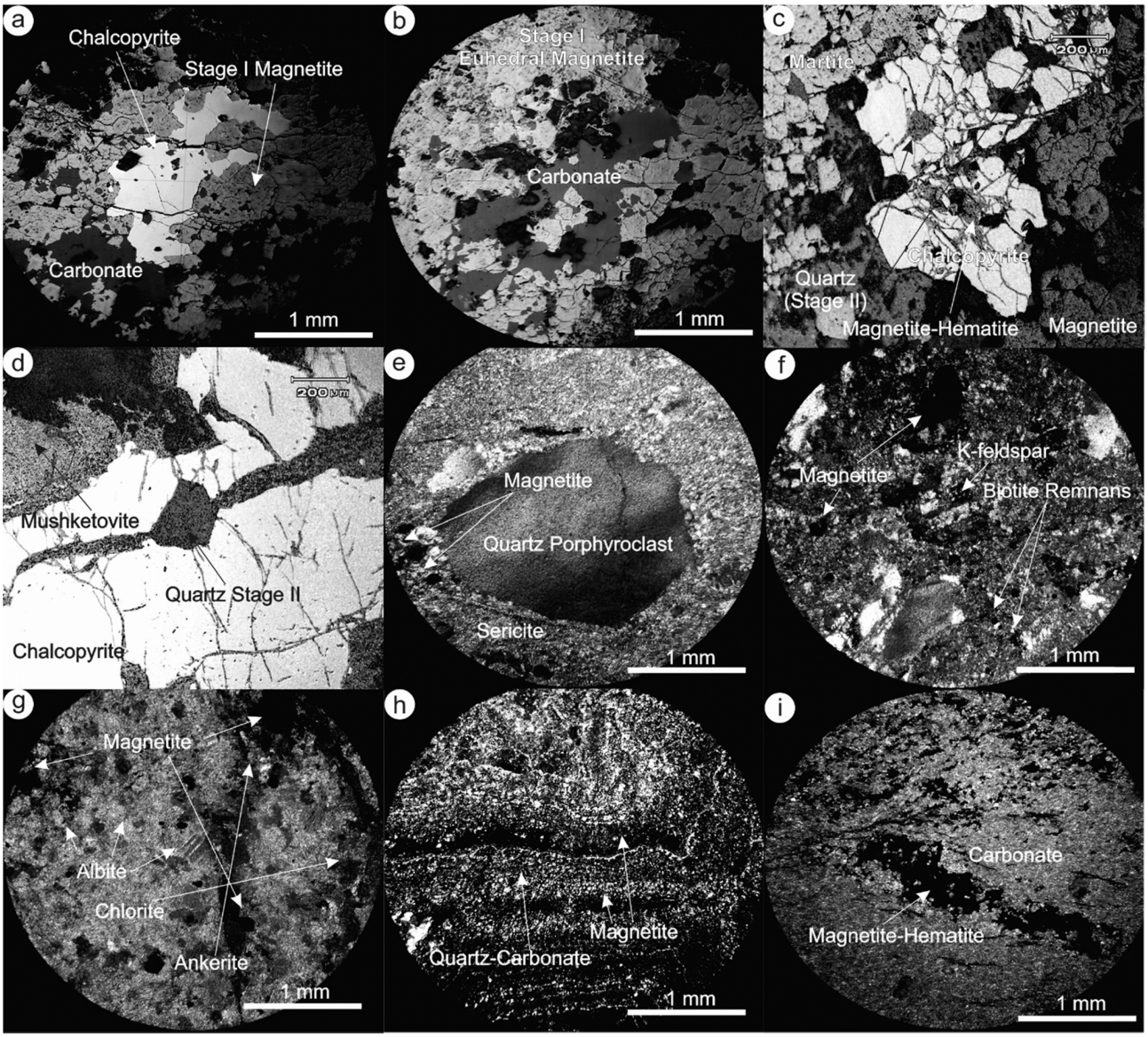

Fig. 5. (a) This figure represents early magnetite and late infill chalcopyrite ore minerals (stage I). The late Fe-oxide and sulfide phases replace the early carbonate phase. (b) Stage I early magnetite phase replaces the carbonate phase. The carbonate minerals occur as un-replaced islands with the ore. (c) The fractured chalcopyrite phase (stage I) is cemented by the early magnetite and late hematite. The late magnetite-hematite (stage I) is transected by the late-stage II quartz mineral. The background magnetite phase is replaced by the hematite phase (martite) (stage I). (d) Fractured chalcopyrite is cemented by the late magnetite-hematite (stage I). The late magnetite-hematite (stage I) is transected by the late-stage II quartz, and magnetite phase (stage I) (mushketovite) replaces the early hematite. (e) quartz-magnetite-carbonate porphyroclast of the mylonitic meta-dolomite. The fine-grained matrix (mylonites) comprises sericite, carbonate, and magnetite. (f) This figure represents the K alteration, affected by the late silicification. This figure represents the replacement of the feldspar phase by the Fe-oxides. The remnant of the biotite and euhedral magnetite occur in the background. (g) This figure represents the mylonitic meta-dolomite with magnetite (black), goethite (black), ankerite (light-grey), albite, and chlorite (dark-grey) mineral assemblage. (h) This figure represents folded ultramylonitic rock with Fe-oxide minerals (black) and light carbonate layers (white). (i) This figure represents magnetite-goethite assemblage (black) in the implosion breccia structure with an ultramylonitic meta-dolomite.

(Fig. 5i). Other open space filling textures such as cavities-vugs, euhedral grains, and replacement texture such as non-matching walls occur within the meta-dolomite as well (Figs. 5d, h and g).

4.1.2. Stage II, III

Stage II and III are characterized by open space filling, replacement, and D_1 deformation textures-structures (Figs. 3d, f, 4b, e, and 5d, h). Stage II is characterized by white to milky euhedral quartz grains as veins, crosscutting stage I mylonitic ore with straight contact (Fig. 4b). This stage highly developed into the ore bodies and meta-dolomite host rock. Replacement textures of stage II comprise pseudomorph, concave surfaces and gradational boundaries (Fig. 3f). The quartz grains of this stage have ~1 cm to several millimeters range in size except for

mylonitic quartz grains, displaying size reduction fabrics (Figs. 5e and h). Also, the D_1 deformation regime affects this stage, displaying vein textured clasts, folding and mylonitic textures-structures (Fig. 3f). Stage III is characterized by abundant hematite and minor magnetite phases (Figs. 3e and 4e). This stage transected stage I–II and highly develops in the peripheral section and through the massive ore bodies as veins with several centimeter widths (Figs. 3d and e). The open space filing and replacement textures of stage III comprise euhedral grains, matching walls and concave surfaces (Fig. 4e). This stage is characterized by folding which is part of the D_1 deformation regime (Fig. 4e).

4.1.3. Stage IV, V

These two stages (Stage IV–V) formed in the brittle deformation regime (D_2), displaying abundant open space filling and minor replacement textures relative to the previously described stages (I–III) (Figs. 4e, f and i). The mineral assemblage of stage IV constitutes early magnetite, late hematite, and last quartz as veins with several centimeter widths (Fig. 4f), displaying open space filling textures including symmetrical banding, matching walls, and fine-grained mineral on the walls and coarser one in the center (Fig. 4f). Replacement textures of this stage consist of gradational boundaries. This stage merely developed into the massive ore bodies without a trace with the meta-dolomite host rock. The magnetite and hematite ore minerals have ~0.1 to ~0.5 mm range in size. Stage V is characterized by quartz, calcite, and barite mineral assemblage as veins and veinlet in the mining area, developing into the ore bodies and meta-dolomite host rock (Figs. 4e and i). The vein and veinlets approximately have 3 to 1 mm range in size. The textures-structures of this stage consist of matching walls, and no offset along the intersecting veins.

4.2. Alterations

Five alteration types, including sodic, Fe, K (potassium feldspar), hydrolytic, and silicification identified in the Heneshk deposit. These alteration types are characterized by their mineral assemblage and a different color in the mining area. The sodic, Fe-rich, K, and hydrolytic alterations are characterized by white-pale green, brown, pinkish, and white colors respectively (Figs. 3b, c, e, 4h, and 5f, g). The sodic and Fe alterations occur as a pre-mineralization stage (Table 1). The K and hydrolytic alterations are accompanied by each mineralization stage (stage I, III, and IV). The silicification fully developed with stage II and IV (Table 1). The highly developed alteration types in the mine are sodic, silicification, and Fe being traced over several hundred meters around the mine (Fig. 2). The K and hydrolytic alterations extend over one-two hundred and fifty meters around ore bodies, respectively (Fig. 2). Also, all alteration types have a close temporal-spatial relationship with deformation arrays in the mine.

4.2.1. Sodic and Fe alterations

The sodic and Fe alterations (Na-Ca-Fe) constitute albite, chlorite, ankerite, goethite, calcite, and hematite mineral phases as replacement forms of the meta-dolomite (Table 1). The mineral assemblage of the Fe alteration comprises goethite and hematite (Table 1). These two alteration types developed as a pre-mineralization stage (Table 1), and their intensity increase toward the center of the shear zone and vicinity of the ore bodies. In some localities in the mine, the intensity of the sodic alteration is characterized by the greenish and white colors of the meta-dolomite due to the more abundant of the chlorite or albite minerals respectively. The Fe alteration is characterized by brown color in the mining area caused by more abundant of the goethite mineral, and its intensity steadily increases toward the vicinity of the ore bodies. Both sodic and Fe-rich alteration types have a close temporal-spatial relationship with D_1 deformation textures-structures similar to the stage I mylonitic ores.

4.2.2. K and hydrolytic alterations

These two alteration types occur with each stage of the mineralization as replacement forms of the host rock. The K alteration mineral assemblage constitutes potassium feldspar (K-feldspar) and sparse biotite, and hydrolytic alteration consists of sericite mineral (Table 1; Figs. 5f and e). Each mineralization stage is characterized by early K and late hydrolytic alterations (Table 1). The early K-feldspar and biotite minerals are altered to sericite and Fe-oxides phases, respectively (Fig. 5f). Both K and hydrolytic alterations with the stage I and III are displaying D_1 deformation textures and structures with a close temporal-spatial relationship with deformation arrays (Fig. 3e). However, the K-rich and hydrolytic alterations with stage IV mineralization occur at the selvage of the mineralized veins, displaying D_2 deformation textures (Table 1). Also, these two alteration types overprinted on the sodic alteration, and albite-chlorite are replaced by sericite and Fe-oxides phases, respectively.

4.2.3. Silicifications

The silicification of the ore and meta-dolomite well developed through to stage II and IV. The early development of this alteration with the ore bodies and host rock occurs with the stage II barren quartz veins. Also, this alteration developed with stage IV mineralization at the selvage of the mineralized veins. The silicification with the meta-dolomite host rock and ore bodies is characterized by fine quartz grains (grain size reduction) and porphyroclasts as well. Also, the overprinting of this alteration on the K and hydrolytic alterations, cause the elimination of the textural evidence.

https://doi.org/10.1007/s12303-019-0050-7

5. ANALYTICAL METHODS

EPMA performs on the thin-polish sections of the Heneshk magnetite ore for obtaining concentrations of the major and trace elements including Si, Al, Fe, Mn, Ti, Mg, V, Cr, Zn, and Ni (Table 2) at Activation Laboratory in Ancaster, Ontario, Canada. Measurements were conducted by JEOL microprobe and electron gun, operated at an accelerating voltage of 15 kV and varying spot size from 5 to 10 microns with ZAF (Z = atomic number correction. A = absorption correction. F = characteristic fluorescence correction) matrix correction on the fifteen magnetite grains (Table 2). Wavelength spectrometers (WDS) are used to detect the X-ray counts from the surface of the samples, and the WDS counts X-rays signals for only one element at a time. The counting times performed for these elements are 30 and 15 seconds for peak and background, respectively. The Smithsonian Magnetite (UNSM 114887) was utilized as a standard in this analysis. The detection limit in this method is ±0.01 wt% (100 ppm). Stoichiometric criteria were used for Fe^{3+} estimation in this method (Table 2).

Sulfur stable isotope analysis was conducted on the representative sulfide minerals. Five chalcopyrite samples were selected from crushed magnetite ore under a binocular microscope by hand picking. Then, these ore samples were pulverized in an agate mortar and sent to the Activation Laboratory (Act Lab), Ancaster, Ontario, Canada for the further analytical procedure. In the lab, pure $BaSO_4$ and sulfide samples were combusted to SO_2 gas under ~10^{-3} torr vacuum and then the gas was inlet directly from the vacuum line to the ion source of a VG 602 Isotope Ratio Mass Spectrometer (Ueda and Krouse, 1986). Quantitative combustion to SO_2 was achieved by mixing 5 mgs of each sulfide sample with 100 mgs mixture of V_2O_5 and SiO_2 (with 1:1 weight ratio). The reaction was carried out at 950 °C for 7 minutes in a quartz glass reaction tube. Pure copper turnings were utilized as a catalyst to ensure the complete conversion of SO_3 to SO_2 gas. Internal Lab Standards (Sea Water $BaSO_4$ and Fisher $BaSO_4$) ran at the beginning and end of each set of samples (typically 25), to normalize the data as well as instrumental errors. In this article, all results are reported in the per mill (‰) notation relative to the international CDT standard. Typically, the precision and reproducibility of this method is better than 0.2 per mill (n = 10 internal lab standards).

6. RESULTS

6.1. Magnetite Mineral Chemistry

EPMA conducted on the fifteen individual magnetite grains from the early Fe-oxide assemblage of the stage I mineralization (Tables 1 and 2). These euhedral magnetite crystals have no sign of compositional zoning, replacement textures (e.g., mushketovite) or mineral inclusions. The concentrations of the SiO_2, Al_2O_3,

Table 2. Major and trace elements Electron probe microanalysis (EPMA) of the fifteen individual magnetite grains

Analyte	SiO_2 (wt%)	TiO_2 (wt%)	Al_2O_3 (wt%)	Cr_2O_3 (wt%)	FeO (wt%)	MgO (wt%)	MnO (wt%)	ZnO (wt%)	NiO (wt%)	V_2O_3 (wt%)	Fe^{+3}	Fe^{+2}	Total
Samples													
H-1	0.81	0.00	0.06	0.01	87.36	0.00	0.05	0.00	0.00	n.d.	74.50	25.33	100.77
H-2	0.92	0.00	0.00	0.04	88.48	0.02	0.02	0.10	0.00	n.d.	74.14	25.06	100.30
H-3	0.51	0.04	0.03	0.00	90.47	0.02	0.05	0.11	0.03	n.d.	73.43	24.51	98.73
H-4	0.66	0.00	0.06	0.00	92.32	0.00	0.00	0.00	0.00	n.d.	68.21	31.59	100.52
H-5	1.09	0.00	0.07	0.00	91.84	0.01	0.00	0.00	0.00	n.d.	68.08	31.57	100.83
H-6	0.68	0.00	0.05	0.03	89.67	0.00	0.04	0.00	0.00	n.d.	73.73	24.77	99.29
H-7	1.60	0.00	0.21	0.00	91.30	0.07	0.00	0.03	0.00	n.d.	67.80	31.46	101.17
H-8	0.28	0.12	0.06	0.00	93.73	0.00	0.00	0.13	0.00	n.d.	68.50	30.72	99.79
H-9	0.04	0.00	0.03	0.00	94.96	0.00	0.11	0.00	0.00	n.d.	68.83	30.87	99.87
H-10	0.11	0.01	0.00	0.00	85.39	0.00	0.14	0.03	0.00	n.d.	75.21	25.75	101.25
H-11	0.44	0.00	0.03	0.00	83.62	0.00	0.00	0.04	0.00	n.d.	66.68	31.76	98.95
H-12	1.12	0.00	0.10	0.00	94.46	0.02	0.00	0.00	0.00	n.d.	68.67	31.61	101.51
H-13	0.2	0.03	0.03	0.00	98.59	0.02	0.14	0.00	0.02	n.d.	69.76	31.20	101.23
H-14	0.36	0.16	0.14	0.00	90.53	0.01	0.01	0.02	0.04	n.d.	67.64	31.31	99.70
H-15	1.47	0.05	0.15	0.06	84.02	0.00	0.00	0.00	0.00	n.d.	66.65	31.61	99.99
Average	0.67	0.03	0.07	0.01	90.45	0.01	0.04	0.03	0.01	–	70.12	29.27	100.26
Maximum	1.60	0.16	0.21	0.06	98.59	0.07	0.14	0.13	0.04	–	75.21	31.76	101.51
Minimum	0.02	0.00	0.00	0.00	83.62	0.00	0.00	0.00	0.00	–	24.51	24.51	98.73

Abbreviation: n.d. = not detected.

FeO, MnO, TiO_2, MgO, V_2O_3, Cr_2O_3, ZnO, and NiO were measured and represented in Table 2. Among these oxides, SiO_2, Al_2O_3, and FeO are consistently detected with the magnetite (Table 2). Conversely, the concentration of the V_2O_3 has not detected, and concentrations of the other oxides including MnO, TiO_2, MgO, Cr_2O_3, ZnO, and NiO are occasionally detected with magnetite (Table 2). The average concentrations of the SiO_2, TiO_2, Al_2O_3, Cr_2O_3, MgO, MnO, ZnO, and NiO are 0.67, 0.03, 0.07, 0.01, 0.01, 0.04, 0.03, and 0.01 wt%, respectively (Table 2). The minimum values of the SiO_2 and FeO oxides are 0.02 and 83.62 wt%, respectively (Table 2). Furthermore, the minimum value of the TiO_2, Al_2O_3, Cr_2O_3, MgO, MnO, ZnO, and NiO is zero (Table 2). In fact, among the fifteen magnetite grains, only several grains have detectable concentrations of these elements (Table 2). Among the fifteen-magnetite, nine grains have concentrations of the Zn and Mg elements (Table 2). Ten, eight, six and four magnetite grains have concentrations of the Mn, Ti, Cr, and Ni elements, respectively (Table 2). In general, these magnetite grains are pure and have low concentrations of the major and minor elements as well.

6.2. Sulfur Stable Isotope Analysis

The metamorphic processes (from low to high metamorphic grades) cannot change or affect the pristine isotopic ratios of the sulfide minerals (Corriveau and Spry, 2014). Based on this, five representative chalcopyrite samples including H_8, H_9, H_{10}, H_{11}, and H_{12} from the stage I mineralization sulfide mineral assemblage (Table 1) were selected for sulfur stable isotope analysis. The mineral isotopic ratios ($\delta^{34}S_{minerals\ (CDT)}$) for H_8, H_9, H_{10}, H_{11}, and H_{12} samples are +41.3, +41.2, +40.8, +40.5, and +41.1 respectively. Based on petrography studies on the Heneshk deposit, sulfate minerals not accompanied stage I sulfide mineral assemblage. In this conditions, the precipitations of the sulfide minerals occur in a reduced condition (Baker and Andrew, 1991; Ohmoto and Goldhaber, 1997; John et al., 2003) with negligible fractionation between sulfide minerals and $\delta^{34}S_{H_2S}$ mineralizaed fluid and we can utilize the $\delta^{34}S_{H_2S} \approx \delta^{34}S_{mineral}$ approximation for calculation the $\delta^{34}S_{H_2S}$ mineralized fluid (Ohmoto and Goldhaber, 1997). Also, in this reduced condition, we can use $\delta^{34}S \approx \delta^{34}S_{H_2S}$ approximation (Ohmoto and Ray, 1997). Therefore, based on two approximation as discuss above, we can use $\delta^{34}S\Sigma S \approx \delta^{34}S_{mineral}$ approximation (Ohmoto and Goldhaber, 1997). Furthermore, the effects of the temperature on the fractionation factor between chalcopyrite and the $\delta^{34}S_{H_2S}$ mineralized fluid is less than 0.7‰ (1000 ln$\propto$) in a temperature range between 0 to 1000 °C (Li and Liu, 2006). So, considering the effect of the temperature, our extended range of $\delta^{34}S_{H_2S(mineralizaed\ fluid)}$ is between 39.8 to 40.6‰.

7. DISCUSSION

7.1. Syn-deformational Mineralization of the Heneshk Deposit

The interpretation of the deformation textures-structures evidence, textural interrelationships, and mineral phase equilibria propose the syn-deformational formation of the ore and gangue minerals in the Heneshk deposit. Based on petrographic studies, there are two types of textural evidence, indicating pre-syn or syn-deformational formation of the ore and gangue minerals. The deformation textures including mylonites, S=C structures, folding, vein textured clasts, rootless folds, and foliation indicate the pre-syn deformational formation of the pre-mineralization stage and stage I–III mineral assemblages. Similarly, these textures including veins textured clasts, and folding of the ore and gangue minerals interpret as pre-syn deformational indicators in Orogenic Gold Deposits (OGDs) (Goldfarb et al., 2005). One of the strong indicators of syn-deformational mineralization is the implosion breccia structures, filling with stage I magnetite. Clearly, the implosion breccia structures are formed during syn-deformational processes (plastic deformation) by a high-pressure fluid, flowed into the opening structure, at the time of formation (in step or in a fault) and minerals begin to precipitate in the structure (Vernon, 2004). In Heneshk deposit, these structures fill with euhedral magnetite (stage I) in the goethite rich matrix, indicating the presence of a high-pressure Fe-rich fluid (mineralized fluid) at the time of the plastic deformation (mylonitization event) causes the formation of the magnetite. Hence, the implosion breccias indicate the syn-deformational mineralization event for stage I mineral assemblage.

The textural interrelationship of the Heneshk deposit including overprinting relationships of the plastic and brittle textures-structures are the identical to the mylonitic terranes, proposing the syn-deformational formation of the deposit during metamorphism. The mylonitic terranes are characterized by overprinted brittle deformation textures-structures on plastic deformation textures-structures (Passchier and Trouw, 2005). Plastic deformation textures-structures including mylonites, S=C structures, folding, implosion breccias, and rootless folds develop in the high temperature-pressure environments with the general characteristic of abundant replacement and scarce open space filling textures (Guilbert and Park, 1986; Vernon, 2004; Passchier and Trouw, 2005). Conversely, in brittle deformation regime, textures including late tensional vein systems develop in the low temperature-pressure environments relative to the plastic deformation with the general characteristic of abundant open space filling and scarce replacement textures (Guilbert and Park, 1986; Vernon, 2004; Passchier and Trouw, 2005). The plastic deformation (D_1) textures-structures with the

https://doi.org/10.1007/s12303-019-0050-7

general characteristic of abundant replacement and scarce open space filling textures and brittle deformation (D_2) textures-structures with the general characteristic of abundant open space filling and scarce replacement textures, in the Heneshk deposit are the identical to the mylonitic terranes. Also, the overprinted brittle (D_2) on the early plastic (D_1) deformation textures-structures in the Heneshk deposit is the identical to the mylonitic terrane. Overall, this identical pattern and consistency between the depositional and deformation textures proposed syn-deformational mineralization in the Heneshk deposit.

Furthermore, another means for investigations of the syn-deformational formation of the Heneshk deposit is mineral phase equilibria interrelationships. The mineral assemblage of the Heneshk deposit can consider as mineral phase equilibria during the metamorphism. From this point of view, the ore and gangue minerals are Silicate-Carbonate-Oxides (SCO) mineral phase equilibria (Eqs. 1–4; Frost, 1991). From the SCO mineral phase equilibria, during metamorphism in greenschist or lower amphibolite facies, different mineral assemblages including greenalite, minnesotaite, grunerite, and fayalite phases can form in the oxidized condition relative to the FMQ (Fayalite-Magnetite-Quartz) buffer similar to the Banded Iron Formation (BIF) with same ore and gangue mineral assemblages (Eqs. 1–4; Frost, 1991). The equations for forming of these mineral phases are represented below. These equations are a series of continuous reactions in which temperature and fO_2 are increase and decrease relative to the FMQ buffer, respectively (Frost, 1991). Based on the SCO mineral phase equilibria, mineral assemblage of the Heneshk deposit, and metamorphic grade in Dehbid district (lower amphibolite facies), mineral phases including greenalite, minnesotaite, grunerite, and fayalite must form in this condition. The absence of these phases indicates that the SCO mineral phases were not coexisting during the prograde metamorphism, to attain an equilibrium. So, mineral assemblage of the Heneshk deposit had not formed before the metamorphic event in late Triassic or in the prograde metamorphism. As discussed below, stage I mineralization formed at 300 °C and 10 km in depth (~2.8 kb) and based on previous studies by Alric and Virlogeus (1977) and Houshmandzadeh et al. (1975), the maximum pressure during peak metamorphism in Dehbid was 5 kb. So, rationally different mineral phases including quartz and clay minerals should form in the different stages (time intervals) without coexisting during the retrograde metamorphism in a decreasing temperature and pressure environment (300 °C and ~2.8 kb). In this condition, different mineral phases have not enough time to achieve a new equilibrium for the formation of the new mineral phases in a decreasing temperature-pressure regime (Eqs. 1–4). So, this result proposes syn-deformational formation and development of the different stages and mineral assemblage in Heneshk deposit in the time interval of the D_1 to D_2 deformation regime during the retrograde metamorphism.

$$6Fe_2O_3\ (\text{Hematite}) + 8SiO_2\ (\text{Quartz}) + 8H_2O\ (\text{vapor}) = 4Fe_3Si_2O_5(OH)_4\ (\text{Greenalite}) + 3O_2, \quad (1)$$

$$2Fe_3O_4\ (\text{Magnetite}) + 8SiO_2\ (\text{Quartz}) + 2H_2O\ (\text{vapor}) = 4Fe_3Si_4O_{10}(OH)_2\ (\text{Minnesotaite}) + 2O_2, \quad (2)$$

$$14Fe_3O_4\ (\text{Magnetite}) + 48SiO_2\ (\text{Quartz}) + 6H_2O\ (\text{vapor}) = 6Fe_7Si_8O_{22}(OH)_2\ (\text{Grunerite}) + 7O_2, \quad (3)$$

$$2Fe_3O_4\ (\text{Magnetite}) + 3SiO_2\ (\text{Quartz}) = 4Fe_2SiO_4\ (\text{Fayalite}) + O_2. \quad (4)$$

7.2. Temperature-Pressure Range during the Mineralization

Based on the textural evidence, overprinting relationships, and mineral phase equilibria, as discussed above, stage I mineralization in the Heneshk deposit formed during the deformational processes (mylonitization event) and retrograde metamorphism. Strong textural evidence such as the deformed quartz-feldspar minerals, quartz recrystallization, and presence of the rare biotite mineral during the mylonitization of the stage I–II can use as a powerful tool to constrain the temperature-pressure range of the mineralization environment during the mylonitization event. Occurrence of the quartz-feldspar grain size reduction in mylonitic terranes indicates that deformation occurs at approximately 300 to 450 °C and 10–15 km in depth (Vernon, 2004) and recrystallization of quartz grains with ~2.8 to ~2.9 μm range in size occur at 300 °C in these terranes during deformation (Passchier and Trouw, 2005). So, textural evidence in Heneshk deposit such as the quartz-feldspar grain size reduction and recrystallization of the quartz grains with approximately 2.8 to ~2.9 μm range in size, as coronas of porphyroclasts indicate that mylonitization-mineralization event should occur at approximately 300 °C and 10–15 km in depth.

Another strong evidence is the presence of comparatively rare biotite as a critical mineral phase of the K-alteration in the stage I mineralization. In one hand, in metamorphic conditions and in an equilibrium involving ferric iron in silicates (biotite) and magnetite-hematite, there is a tendency for partitioning of Fe^{3+} in magnetite-hematite into the silicates, at the expense of these oxides without any change in the oxidation state (Frost, 1991). On the other hand, the occurrence of the rare biotite in Heneshk deposit reflects the lack of partitioning of Fe^{3+} in the biotite as the expense of the magnetite-hematite ore in the retrograde metamorphism (stage I). Also, in OGDs, biotite begins to emerge in mineral assemblages at approximately 300 °C and 10 km in depth (~2.8 kb) (Groves, 1993). According to the partitioning and emerging of the biotite, it is rational that the ideal environment (temperature-pressure range) for the growth of the biotite (stage

I alteration facies) as the expense of the magnetite-hematite ore was not provided and it was at the edge of the temperature range for biotite formation (300 °C). As a result, we consider the temperature-pressure range of the stage I mineralization environment in the Heneshk deposit at approximately 300 °C and 10 km in depth.

7.3. Magnetite Mineral Chemistry of the Heneshk Deposit

The magnetite mineral chemistry of the stage I mineralization, economically the most critical stage, in the Heneshk deposit (more than 95 vol. percent of the ore bodies) is in accordance with metamorphic magnetite. We use a modified Dupuis and Beaudoin (2011) diagram by Nadoll et al. (2014), to compare the mineral chemistry of the Heneshk deposit with other deposit types. Six magnetite grains with elemental concentrations of the Ti, Al, and Mn (H_3, H_8, H_{10}, H_{13}, H_{14}, and H_{15}; Table 2; Fig. 6) are plotted on the diagram. The data with zero value were not utilized for this comparison due to the unacceptable results on the diagram (Table 2). The designated area of these points on the diagram is in accordance with IOCGs and BIFs (Fig. 6). Furthermore, the upper, lower, and average elemental concentrations of the Mg, Al, Ti, Ni, Cr, Mn, and Zn are plotted on the diagram, proposed by Nadoll et al. (2014) for distinguishing the different hydrothermal magnetite types (Fig. 7). The average concentrations of all elements

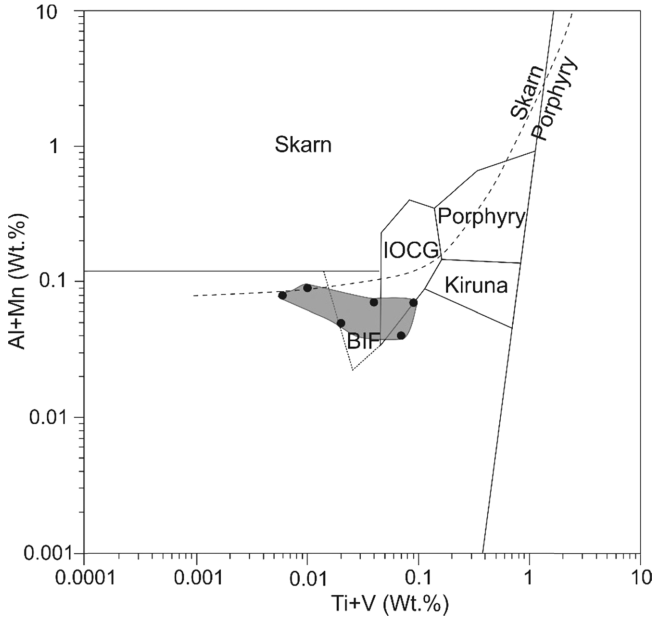

Fig. 6. The EPMA of the Heneshk magnetite deposit are plotted on the modified diagram of the Dupuis and Beaudoin (2011) by Nadoll et al. (2014). The location of the six analyses of the Heneshk magnetite (stage I) with elemental concentrations of the Ti, Al, and Mn (H_3, H_8, H_{10}, H_{13}, H_{14}, and H_{15}) are displayed on the diagram. Other data cannot plot on the diagram due to the zero values of the Ti, Al, and Mn elements.

are in accordance with Ag, Pb, Zn hydrothermal magnetite, representing the metamorphic magnetite (Fig. 7). The Ag, Pb, Zn hydrothermal magnetite is represented the occurrence of the magnetite in Coeur d' Alene mining district, Idaho, USA, during the metamorphic event (Leach et al., 1988; Constantopoulos, 1994; Eaton et al., 1995; Fleck et al., 2002; Nadoll et al., 2014). The lower limits for elemental concentrations of the Heneshk magnetite merely can compare with BIFs due to the very low concentrations of these elements (zero value) (Fig. 7). In general, the elemental concentrations of the Heneshk magnetite are very low, and we can consider the Heneshk magnetite as a pure magnetite. Only metamorphic magnetite is too pure and has very low elemental concentrations, especially for the Ti element (Frost, 1991). So, economically-volumetrically, the most critical mineralization stage in Heneshk deposit (Stage I) is in accordance with the metamorphic magnetite and IOCG, and due to the very low elemental concentrations, it has an overlap with BIFs magnetite as well.

7.4. Partitioning of Elements in Magnetite Phase during Mylonitization

As discuss above, the Heneshk magnetite mineral chemistry of the stage I mineralization only can compare with the Ag, Pb, Zn hydrothermal magnetite and due to the very low elemental concentrations, the quantitative data on this magnetite have a considerable overlap with BIFs magnetite in the Dupuis and Beaudoin (2011) and Nadoll et al. (2014) diagrams. This overlap can explain by Dare et al. (2014) diagrams, classifying magnetite based on temperature ranges of mineralized fluids. These temperature ranges, control of the elemental substitutions cause for fairly similar elemental concentrations in one group (Dare et al., 2014). The Ag, Pb, Zn, hydrothermal and BIF magnetite are classified by Dare et al. (2014) as the low-temperature magnetite, forming with a maximum temperature limit of 300 °C with fairly similar elemental concentrations. As discussed above, stage I mineralization of the Heneshk deposit approximately formed in the 300 °C, similar to the Ag, Pb, Zn hydrothermal magnetite during metamorphism. So, we expect similar elemental concentrations for the Heneshk magnetite and the BIF as well. However, maximum elemental concentrations for the Ni, Cr, Zn, Al, and slightly Ti are high and can compare with the magmatic-hydrothermal magnetite. Elements such as Ni, Cr, and Zn with higher concentrations are the most compatible elements in magnetite mineral structure and their substitution mainly control over a change in the temperature ranges between different geological environments (Dare et al., 2014; Nadoll et al., 2014). Therefore, by considering the temperature range of the stage I mineralization in Heneshk deposit (300 °C, low-temperature environment)

https://doi.org/10.1007/s12303-019-0050-7

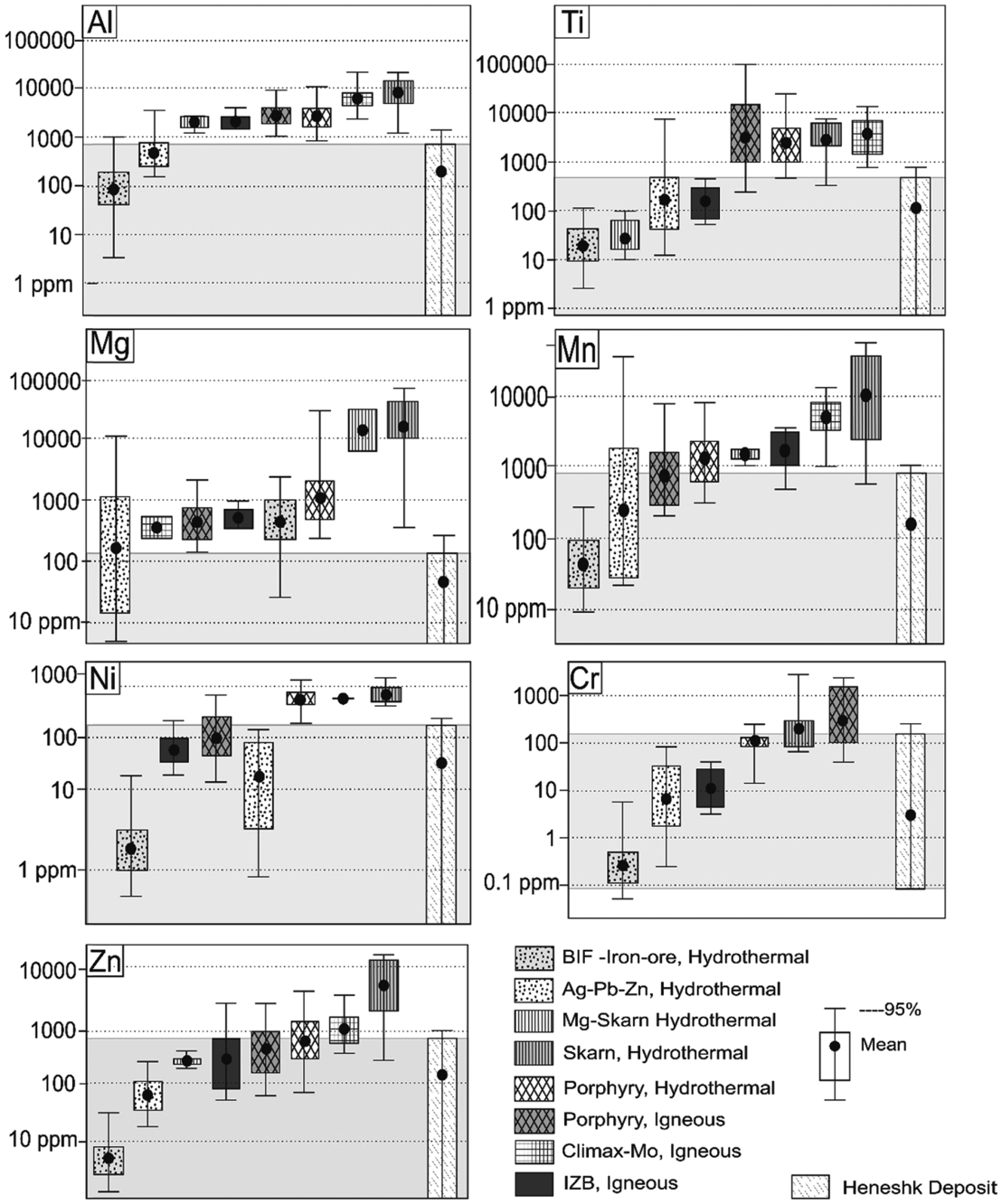

Fig. 7. The EPMA data of the Heneshk magnetite deposit are plotted on the Nadoll et al. (2014) diagram.

and proposed elemental concentrations for the magnetite in this temperature range by Dare et al. (2014) and Nadoll et al. (2014), the higher elemental concentrations of the Ni, Cr, Zn, Ti, and Al can relate to the higher pressure (10 km in depth, ~2.8 kb) of the mineralization environment. This higher elemental concentration may indicate the higher pressure of the mineralization environment lead to the higher elemental substitutions in magnetite mineral structure, especially for the most compatible elements in magnetite structure such as Ni, Cr, and Zn. Also, the incompatible elements in the magnetite structure, such as Si (Dare et al., 2014) should have a lower concentration relative to the compatible elements, even in a high-pressure environment. However, the Heneshk deposit recorded the highest concentrations of the Si element as well. These concentrations only can compare with skarn magnetite deposits (0.1–6 wt% Si) with unknown substitution mechanism for this element (Dare et al., 2014). It is possible the Si concentration also related to the higher pressure of the mineralization environment as we proposed for other relatively compatible elements. Finally, the unusual lack of any traceable concentrations of V element possibly related to the

primary low concentration of this element in the mineralized fluid as well.

7.5. Source of the Sulfur and Precipitation Mechanism

Based on the sulfur stable isotope data, paleo-evaporates are only sources of the sulfur component of the Heneshk deposit with Thermochemical Sulfate Reduction (TSR) mechanism for mineral precipitations. The $\delta^{34}S_{H_2S(mineralizaed\ fluid)}$ of the Heneshk deposit is between +39.8 to +40.6‰. In fact, this range is heavier than any paleo-evaporates ever formed through the geological time from the sea water sulfate (~+34‰, reported by Claypool et al., 1980). Therefore, the sulfide minerals such as chalcopyrite and pyrite must form through a very specific precipitation mechanism from a sulfate source. Isotopically, only TSR mechanism can explain that the generation of the heavier sulfide minerals from a relatively heavy sulfate source (Ohmoto and Goldhaber, 1997; Peevler et al., 2003). So, the sulfide minerals in the Heneshk deposit must form from a sulfate source by TSR mechanism. These paleo-evaporates must leached from the older rock strata in Dehbid region including the Silurian or upper Devonian–Lower Carboniferous rock sequences. In conclusion, the sulfur component in the Heneshk deposit does not relate to none of the magmatic source or syngenetic deposits such as BIFs due to the heavier sulfur source than sea water sulfate.

7.6. Constraint on Genesis of the Heneshk Deposit

Different geological line of evidence in the Heneshk deposit including the textural evidence, the SCO mineral phase equilibria, the magnetite mineral chemistry, and the contribution of the paleo-evaporates are in accordance with a metamorphogenic ore. Evidence such as the implosion breccia textures-structures, the sulfur isotope data, and the magnetite mineral chemistry indicate that the stage I mineralization formed during the metamorphism in late Triassic. This stage constitutes more than 95 volume percent of the ore bodies cause of the present value of this deposit, economically. The approval of this genesis for the stage I mineralization has two important consequences: (1) Stage III mineralization is part of the D_1 deformation regime identical to the stage I mineralization with a metamorphic origin during an ongoing deformation regime. (2) The stage IV mineralization with the same ore mineralogy and the alteration types similar to the stage I and III mineralization formed in the retrograde metamorphism after the D_1 deformation regime in a tensional tectonic regime (the D_2 deformational regime). In conclusion, mineralization in the Heneshk deposit occurred in a deformation regime during the metamorphic event in the late Triassic in Dehbid district.

Furthermore, the critical genetic aspects of the Heneshk deposit including the source of the mineralized fluid, the fluid convection, and the possibility of the mass transfer in a metamorphic environment and a shear zone should occur in a similar way to the proposed mechanisms for forming new mineral phases in a metamorphic environment. The mineralized fluid in the Heneshk deposit during the metamorphism should have originated from the Silurian and upper Devonian–Lower Carboniferous strata caused by the physical (e.g., dewatering of the pore water) and chemical devolatilization of the pore fluids, clay minerals, carbonates, and other possible sources. The physical and chemical devolatilizations are the main mechanisms for producing fluids in metamorphic environments from rock sequences (Roedder, 1984). Presumably, the generated mineralized fluid, actively circulated through the pile of the rock sequences and the shear zone, forming the Heneshk mineral assemblage during metamorphism by leaching the ore components from rock strata. The presence of the active or less active circulated fluids into the shear zone is proposed by Etheridge et al. (1983) and other studies indicate the considerable mass transfer in shear zones during metamorphism (Vernon, 2004). So, based on the proposed mechanisms for forming new minerals in metamorphic environments, the occurrence of the Heneshk mineral assemblages and critical genetic aspects of the mineralization can fully justify during the metamorphic event in Dehbid district.

7.7. Commonalities of the Heneshk Deposit with IOCGs

The Heneshk Fe ± Cu deposit has the unequivocal geological key characteristics of IOCGs. The first, IOCGs have structural controls on mineralization (Williams et al., 2005; Groves et al., 2010; Barton, 2014) and they are stratabound in nature (Barton, 2014). Mineralization in the Heneshk deposit including two ore bodies and concomitant alterations bound to the meta-dolomite host rock and a shear zone as stratabound ore bodies and paragenetic stages are displaying temporal-spatial relationships with deformation arrays (D_1, D_2) in a shear zone, reflecting structural controls on the mineralization. In the second place, the transforming extensional tectonic setting or extensional tectonic regime into the compressional tectonic regime (e.g., Andean IOCGs) is considered as a frequent tectonic setting for IOCGs and these deposits are accompanied by the coeval magmatism (bimodal volcanism and intrusions) (Groves et al., 2010; Barton, 2014) (e.g., felsic intrusions in the South Australia, Pollard, 2006 and SE Missouri, Nold et al., 2014). The tectonic setting of the Heneshk deposit was a rifting setting, transformed to a continental magmatic arc (compressional tectonic regime) during the Late Carboniferous to early Jurassic time interval (Berberian and King, 1981; Verdel et al., 2011; Alirezaei and Hassanzadeh, 2012; Richards, 2015; Davoudian et al., 2016; Hassanzadeh and Wernicke, 2016)

https://doi.org/10.1007/s12303-019-0050-7

similar to the IOCGs. Also, the characteristic of this time interval in Dehbid district is bimodal volcanism and coeval A type felsic intrusions with the Kowli-Kosh complex similar to the IOCGs. Moreover, the mineralogy and magnetite geochemistry of the IOCGs and Heneshk deposit are similar in every aspect. IOCGs contain low Ti (< 1 wt%) abundant magnetite-hematite (namely specularite) with abundant chalcopyrite and pyrite as common sulfide phases (Williams et al., 2005; Groves et al., 2010; Barton, 2014). Also, some authors reported the presence of the mushketovite with some typical and world-class IOCGs (e.g., Oak Dam, Davidson et al., 2007; Raul-Condestable, De Haller and Fontbote, 2009; Marcona-Mina Justa, Chen et al., 2010; Mantoverde, Rieger et al., 2010; Domingo, Daroch and Barton, 2011; Hamlin lake, Forslund, 2012; deposits in Purcell rage, Galicki et al., 2012; El Espino, Lopez et al., 2014) and others mentioned that mineral phase as well (e.g., Williams et al., 2005 ; Chen, 2013; Barton, 2014). The ore mineralogy of the Heneshk deposit comprises abundant low Ti-magnetite (Table 2), chalcopyrite, minor hypogene martite, mushketovite, and hematite (specularite) (Table 1) as the same as IOCGs. Another critical characteristic of the IOCG deposit is the hydrothermal nature of the mineralization, alkali metasomatism (Na-Ca), hydrolytic (acid, H^+), and K-rich alteration types (Hitzman et al., 1992; Williams et al., 2005; Groves et al., 2010; Barton, 2014). The replacement and open space filling textures reflect the hydrothermal nature of mineralization (e.g., Guilbert and Park, 1986; Taylor, 2009) and these textures are most typical characteristics of the mineralization stages in the Heneshk deposit. Also, the pre-mineralization sodic, simultaneous K and hydrolytic alterations in the Heneshk deposit are identical to IOCGs. Furthermore, another essential characteristic of the IOCGs is oxidized host rock (Barton, 2014). The pre-mineralization Fe alteration of the Heneshk deposit oxidized the meta-dolomite host rock similar to the IOCGs. Finally, some of the world class IOCGs have a deep crustal setting such as Cloncurry district, Australia (Williams et al., 2005) and the Heneshk deposit has a similar deep-seated setting. In conclusion, the Heneshk deposit and IOCGs are similar in key aspects including the structural controls on mineralization, stratabound nature of the mineralization, rifting setting transformed to continental magmatic arc, coeval magmatism, mineralogy, magnetite mineral geochemistry, hydrothermal nature of mineralization, alteration facies, oxidize host rock, and mineralization in the deep crustal setting (10 km in depth).

8. CONCLUSION

During the last decade, most of the researchers propose magmatic origins for the most IOCGs and their concomitant alteration types, worldwide. Among these studies, the role of metamorphism in ore-forming processes for IOCGs receives scant attention due to the sparse geological evidence, supporting this role. The line of evidence, supporting the contribution of the metamorphic ore-forming components was established on the stable or radiogenic isotopic data on the coexist mineral phase with the ore such as quartz or sulfide minerals on a few deposits and even is these cases, the contribution of the magmatic components was always recorded. The mineral chemistry of the magnetite usually does not recognizes as a means for explorational targeting for IOCGs. Also, the most IOCGs are hosted by the metamorphic terrane around the world, and the geological ore-forming environments for the most IOCGs did not constrain, due to the difficulties of unraveling the time interrelationships of the mineralization and metamorphic event.

Based on the magnetite mineral chemistry, sulfur isotope data, and textural evidence, the Heneshk IOCG deposit is a metamorphogenic deposit and formed in the late Triassic metamorphic event in deep-seated rocks. Our investigation does not support any magmatic contributions in the critical ore-forming event in this deposit (stage I). In other words, the metamorphic processes can consider as the critical ore-forming processes in the IOCGs. Also, the Heneshk IOCG deposit has the most common key characteristics of the Andean IOCG deposit such as mineral species and alteration types. However, the Andean IOCG mostly related to the magmatic processes rather than a metamorphic one. Our investigation reveals the role of metamorphic processes in the formation of the sodic, K-rich and hydrolytic alterations in the Andean IOCG type. Further, our diagnostic textural evidence such as implosion breccia and temporal-spatial relationships with deformation arrays had not utilized before to constraint the genetic aspects and ore-forming environments for other IOCGs, worldwide. So, the textural evidence can utilize for unraveling the time relationships of mineralization event and constrain the ore-forming environment in other IOCGs with the metamorphosed host rock, worldwide.

Finally, our investigation represents the first mineral chemical signature of low temperature-high pressure metamorphic magnetite and mineral chemical behavior of the most and relatively least compatible elements (Ni, Cr, Zn, Ti, Al, and Si) in such an environment. Finally, despite the very low Ti and high Si concentrations of the mineral chemistry, the Heneshk magnetite signature can utilize for distinguishing the fertile or barren IOCGs in the metamorphic terranes in mineral exploration as well.

ACKNOWLEDGMENTS

This project including EPMA, sulfur stable isotope analysis, and field studies are funded by the personal asset of the author (Mr. Mizan). We like to thanks professor J.L. Nold for reviewing the early version of this manuscript and Mr. Razfar from Iron

Madkansar Company for accessing to the mine. Also, we thank N. Oksuz and an unknown reviewer for their thoughtful comments, aiding us to improve the manuscript.

REFERENCES

Alirezaei, S. and Hassanzadeh, J., 2012, Geochemistry and zircon geochronology of the Permian A-type Hasanrobat granite, Sanandaj-Sirjan belt: a new record of the Gondwana break-up in Iran. Lithos, 151, 122–134.

Alric, G. and Virlogeus, D., 1977, Petrography and geochemistry study of metamorphic and magmatic in Dehbid-Bavanat region. Ph.D. Thesis, Geological Survey of Iran, Tehran, 129 p.

Baker, E.M. and Andrew, A.S., 1991, Geologic, fluid inclusion, and stable isotope studies of the gold-bearing breccia pipe at Kidston, Queensland, Australia. Economic Geology, 86, 810–830.

Barton, M.D., 2014, Iron oxide (Cu-Au-REE-P-Ag-U-Co) systems. In: Holland, H.D. and Turekian, K.K. (eds.), Treatise on the Geochemistry, Volume 13: Geochemistry of Mineral Deposits. Elsevier, Amsterdam, p. 515–541.

Berberian, M. and King, G.C.P., 1981, Towards a paleogeography and tectonic evolution of Iran. Canadian Journal of Earth Sciences, 18, 210–265.

Chen, H., 2013, External sulphur in IOCG mineralization: implications on definition and classification of the IOCG clan. Ore Geology Reviews, 51, 74–78.

Chen, H., Clark, A.H., Kyser, T.K., Ullrich, T.D., Baxter, R., Chen, Y., and Moody, T.C., 2010, Evolution of the giant Marcona-Mina Justa iron oxide-copper-gold district, south-central Peru. Economic Geology, 105, 155–185.

Claypool, G.E., Holser W.T., Kaplan, I.R., Sakai, H., and Zak, I., 1980, The age curves of sulfur and oxygen isotopes in marine sulfate and their mutual interpretation. Chemical Geology, 28, 199–260.

Constantopoulos, J., 1994, Oxygen isotope geochemistry of the Coeur d'Alene mining district, Idaho. Economic Geology, 89, 944–951.

Corriveau, L. and Spry, P.G., 2014, Metamorphosed hydrothermal ore deposits. In: Holland, H.D. and Turekian, K.K. (eds.), Treatise on the Geochemistry, Volume 13: Geochemistry of Mineral Deposits. Elsevier, Amsterdam, p. 175–194.

Dare, S.A., Barnes, S.J., Beaudoin, G., Méric, J., Boutroy, E., and Potvin-Doucet, C., 2014, Trace elements in magnetite as petrogenetic indicators. Mineralium Deposita, 49, 785–796.

Daroch, G.A. and Barton, M.D., 2011, Hydrothermal alteration and mineralization in Santo Domingo Sur iron oxide (Cu-Au) (IOCG) deposit, Atacama region, Chile. 11th Society for Geology Applied to Mineral Deposits Biennial Meeting "Let's Talk Ore Deposits" (Expanded Abstract), Antofagasta, Chile, Sep. 26–29, p. 635–637.

Davidson, G.J., Paterson, H., Meffre, S., and Berry, R.F., 2007, Characteristics and origin of the Oak Dam East breccia-hosted, iron oxide Cu-U-(Au) deposit: Olympic Dam region, Gawler craton, South Australia. Economic Geology, 102, 1471–1498.

Davoudian, A.R., Genser, J., Neubauer, F., and Shabanian, N., 2016, $^{40}Ar/^{39}Ar$ mineral ages of eclogites from North Shahrekord in the Sanandaj-Sirjan Zone, Iran: implications for the tectonic evolution of Zagros orogen. Gondwana Research, 37, 216–240.

De Haller, A. and Fontboté, L., 2009, The Raúl-Condestable iron oxide copper-gold deposit, central coast of Peru: ore and related hydrothermal alteration, sulfur isotopes, and thermodynamic constraints. Economic Geology, 104, 365–384.

Dupuis, C. and Beaudoin, G., 2011, Discriminant diagrams for iron oxide trace element fingerprinting of mineral deposit types. Mineralium Deposita, 46, 319–335.

Eaton, G.F., Criss, R.E., Fleck, R.J., Bond, W.D., Cleland, R.W., and Wavra, C.S., 1995, Oxygen, carbon, and strontium isotope geochemistry of the Sunshine Mine, Coeur d'Alene mining district, Idaho. Economic Geology, 90, 2274–2286.

Etheridge, M.A., Wall, V.J., and Vernon, R.H., 1983, The role of the fluid phase during regional metamorphism and deformation. Journal of Metamorphic Geology, 1, 205–226.

Fergusson, C.L., Nutman, A.P., Mohajjel, M., and Bennett, V.C., 2016, The Sanandaj-Sirjan zone in the Neo-Tethyan suture, western Iran: zircon U-Pb evidence of late Palaeozoic rifting of northern Gondwana and mid-Jurassic orogenesis. Gondwana Research, 40, 43–57.

Fleck, R.J., Criss, R.E., Eaton, G.F., Cleland, R.W., Wavra, C.S., and Bond, W.D., 2002, Age and origin of base and precious metal veins of the Coeur d'Alene mining district, Idaho. Economic Geology, 97, 23–42.

Forslund, N., 2012, Alteration and fluid characterization of the Hamlin Lake IOCG occurrence, northwestern Ontario, Canada. M.Sc. Thesis, University of Lakehead, Thunder Bay, Canada, 285p.

Frost, B.R., 1991, Magnetic petrology: factors that control the occurrence of magnetite in crustal rocks. Reviews in Mineralogy and Geochemistry, 25, 489–509.

Galicki, M., Marshall, D., Staples, R., Thorkelson, D., Downie, C., Gallagher, C., Enkin, R., and Davis, W., 2012, Iron oxide ± Cu ± Au deposits in the Iron Range, Purcell Basin, southeastern British Columbia. Economic Geology, 107, 1293–1301.

Goldfarb, R., Baker, T., Dube, B., Groves, D.I., Hart, C.J., and Gosselin, P., 2005, Distribution, character and genesis of gold deposits in metamorphic terranes. In: Hedenquist, J.W., Thompson, J.F.H., Goldfarb, R.J., and Richards, J.P. (eds.), Economic Geology 100th Anniversary Volume (1905–2005). Society of Economic Geologist, Colorado, p. 407–450.

Groves, D.I., 1993, The crustal continuum model for late-Archaean lode-gold deposits of the Yilgarn Block, Western Australia. Mineralium Deposita, 28, 366–374.

Groves, D.I., Bierlein, F.P., Meinert, L.D., and Hitzman, M.W., 2010, Iron oxide copper-gold (IOCG) deposits through Earth history: implications for origin, lithospheric setting, and distinction from other epigenetic iron oxide deposits. Economic Geology, 105, 641–654.

Guilbert, J.M. and Park, C.F., Jr., 1986, The Geology of Ore Deposits (3rd edition). W.H. Freeman, New York, 985 p.

Hassanzadeh, J. and Wernicke, B.P., 2016, The Neotethyan Sanandaj–Sirjan zone of Iran as an archetype for passive margin-arc transitions. Tectonics, 35, 586–621.

Hitzman, M.W., Oreskes, N., and Einaudi, M.T., 1992, Geological characteristics and tectonic setting of Proterozoic iron oxide (Cu-U-Au-REE) deposits. Precambrian Research, 58, 241–287.

Houshmandzadeh, A.R., Ohanian, T., Sahandi, M.R., Taraz, H., Aganabati, A., Soheili, M., and Hamdi, B., 1975, Geological map of Eglid Quadran-

 https://doi.org/10.1007/s12303-019-0050-7

gle (1: 250000). Report N.10, Geological Survey of Iran, Tehran, 165 p.

Huang, X.W., Boutroy, E., Makvandi, S., Beaudoin, G., Corriveau, L., and De Toni, A.F., 2018, Trace element composition of iron oxides from IOCG and IOA deposits: relationship to hydrothermal alteration and deposit subtypes. Mineralium Deposita, 54, 525–552. https://doi.org/10.1007/s00126-018-0825-1

John, D.A., Hofstra, A.H., Fleck, R.J., Brummer, J.E., and Saderholm, E.C., 2003, Geologic setting and genesis of the Mule Canyon low-sulfidation epithermal gold-silver deposit, north-central Nevada. Economic Geology, 98, 425–464.

Leach, D.L., Landis, G.P., and Hofstra, A.H., 1988, Metamorphic origin of the Coeur d'Alene base-and precious-metal veins in the belt basin, Idaho and Montana. Geology, 16, 122–125.

Lopez, G.P., Hitzman, M.W., and Nelson, E.P., 2014, Alteration patterns and structural controls of the El Espino IOCG mining district, Chile. Mineralium Deposita, 49, 235–259.

Mohajjel, M., Fergusson, C.L., and Sahandi, M.R., 2003, Cretaceous–Tertiary convergence and continental collision, Sanandaj–Sirjan zone, western Iran. Journal of Asian Earth Sciences, 21, 397–412.

Nabatian, G., Rastad, E., Neubauer, F., Honarmand, M., and Ghaderi, M., 2015, Iron and Fe-Mn mineralisation in Iran: implications for Tethyan metallogeny. Australian Journal of Earth Sciences, 62, 211–241.

Nadoll, P., Angerer, T., Mauk, J.L., French, D., and Walshe, J., 2014, The chemistry of hydrothermal magnetite: a review. Ore Geology Reviews, 61, 1–32.

Nadoll, P., Mauk, J.L., Hayes, T.S., Koenig, A.E., and Box, S.E., 2012, Geochemistry of magnetite from hydrothermal ore deposits and host rocks of the Mesoproterozoic Belt Supergroup, United States. Economic Geology, 107, 1275–1292.

Nold, J.L., Dudley, M.A., and Davidson, P., 2014, The Southeast Missouri (USA) Proterozoic iron metallogenic province-types of deposits and genetic relationships to magnetite-apatite and iron oxide-copper-gold deposits. Ore Geology Reviews, 57, 154–171.

Ohmoto, H. and Goldhaber, M.B., 1997, Sulfur and carbon isotopes. In: Barnes, H.D. (ed.), Geochemistry of Hydrothermal Ore Deposits. John Wiley and Sons Inc. New York, p. 517–612.

Passchier, C.W. and Trouw, R.A., 2005, Microtectonics (2rd edition). Springer, Berlin, 366 p.

Peevler, J., Fayek, M., Misra, K.C., and Riciputi, L.R., 2003, Sulfur isotope microanalysis of sphalerite by SIMS: constraints on the genesis of Mississippi valley-type mineralization, from the Mascot-Jefferson City district, East Tennessee. Journal of Geochemical Exploration, 80, 277–96.

Pollard, P.J., 2006, An intrusion-related origin for Cu-Au mineralization in iron oxide-copper-gold (IOCG) provinces. Mineralium Deposita, 41, 179–187.

Rajabzadeh, M.A. and Rasti, S., 2017, Investigation on mineralogy, geochemistry and fluid inclusions of the Goushti hydrothermal magnetite deposit, Fars Province, SW Iran: a comparison with IOCGs. Ore Geology Reviews, 82, 93–107.

Richards, J.P., 2015, Tectonic, magmatic, and metallogenic evolution of the Tethyan orogen: from subduction to collision. Ore Geology Reviews, 70, 323–345.

Rieger, A.A., Marschik, R., Diaz, M., Holzl, S., Chiaradia, M., Akker, B., and Spangenberg, J.E., 2010, The hypogene iron oxide copper-gold mineralization in the Mantoverde district, northern Chile. Economic Geology, 105, 1271–1299.

Roedder, E., 1984, Fluid Inclusions. Reviews in Mineralogy, Volume 12, Mineralogical Society of America, 646 p.

Sabzehei, M., Mirzaei, H., and Mostafavi, M., 2013, Petrographic evidences for the origin of iron in IOCG iron deposits of Kuh-E-Faryadoon and Kouli-Kosh, southeast Central Iran. Journal of Sciences, 24, 41–53.

Samani, B., 2017, Deformation flow analysis and symmetry of Goushti shear zone, Sanandaj-Sirjan metamorphic belt, Iran. Geopersia, 7, 117–130.

Sarkarinejad, K. and Azizi, A., 2008, Slip partitioning and inclined dextral transpression along the Zagros Thrust System, Iran. Journal of Structural Geology, 30, 116–136.

Shahidi, A., Taraz, H., and Zamani Pedram, M., 1999, Geological report of the Dehbid Sheet (1:100,000). Geological Survey of Iran, Tehran, 165 p.

Shanks, W.P.C., 2014, Stable isotope geochemistry of mineral deposits. In: Holland, H.D. and Turekian, K.K. (eds.), Treatise on the Geochemistry, Volume 13: Geochemistry of Mineral Deposits. Elsevier, Amsterdam, p. 59–85.

Taylor, R., 2010, Ore Textures. Springer, Berlin, 288 p.

Ueda, A. and Krouse, H.R., 1986, Direct conversion of sulphide and sulphate minerals to SO_2 for isotope analyses. Geochemical Journal, 20, 209–212.

Verdel, C., Wernicke, B.P., Hassanzadeh, J., and Guest, B., 2011, A Paleogene extensional arc flare-up in Iran. Tectonics, 30. https://doi.org/10.1029/2010TC002809

Vernon, R.H., 2004, A Practical Guide to Rock Microstructure (1st edition). Cambridge University Press, Cambridge, 446 p.

Williams, P.J., Barton, M.D., Johnson, D.A., Fontboté, L., De Haller, A., Mark, G., Oliver, N.H., and Marschik, R., 2005, Iron oxide copper-gold deposits: geology, space-time distribution, and possible modes of origin. In: Hedenquist, J.W., Thompson, J.F.H., Goldfarb, R.J., and Richards, J.P. (eds.), Economic Geology 100th Anniversary Volume (1905–2005). Society of Economic Geologist, Colorado, p. 371–405.